Analysis of Saturation Transfer Electron Paramagnetic Resonance Spectra of a Spin-Labeled Integral Membrane Protein, Band 3, in Terms of the Uniaxial Rotational Diffusion Model

Eric J. Hustedt and Albert H. Beth
Department of Molecular Physiology and Biophysics, Vanderbilt University, Nashville, Tennessee, USA

ABSTRACT Algorithms have been developed for the calculation of saturation transfer electron paramagnetic resonance (ST-EPR) spectra of a nitroxide spin-label assuming uniaxial rotational diffusion, a model that is frequently used to describe the global rotational dynamics of large integral membrane proteins. One algorithm explicitly includes terms describing Zeeman overmodulation effects, whereas the second more rapid algorithm treats these effects approximately using modified electron spin-lattice and spin-spin relaxation times. Simulations are presented to demonstrate the sensitivity of X-band ST-EPR spectra to the rate of uniaxial rotational diffusion and the orientation of the nitroxide probe with respect to the diffusion axis. Results obtained by using the algorithms presented, which are based on the transition-rate formalism, are in close agreement with those obtained by using an eigenfunction expansion approach. The effects of various approximations used in the simulation algorithms are considered in detail. Optimizing the transition-rate formalism to model uniaxial rotational diffusion results in over an order of magnitude reduction in computation time while allowing treatment of nonaxial A- and g-tensors. The algorithms presented here are used to perform nonlinear least-squares analyses of ST-EPR spectra of the anion exchange protein of the human erythrocyte membrane, band 3, which has been affinity spin-labeled with a recently developed dihydrostilbene disulfonate derivative, [^{15}N,$^{2}H_{13}$]-SL-H_2DADS-MAL. These results suggest that all copies of band 3 present in intact erythrocytes undergo rotational diffusion about the membrane normal axis at a rate consistent with a band 3 dimer.

INTRODUCTION

Saturation transfer electron paramagnetic resonance (ST-EPR) spectroscopy of nitroxide spin-labeled biological molecules has been widely applied to the investigation of rotational dynamics on the microsecond to millisecond time scale (Hyde and Dalton, 1972; Thomas and McConnell, 1974; Thomas et al., 1976; Hyde and Dalton, 1979; Dalton, 1985; Hemminga and de Jager, 1989). The technique has the potential to provide detailed information on the rate of rotational diffusion, the anisotropy of the diffusion process, and the orientation of the nitroxide probe with respect to the diffusion tensor (Beth et al., 1983; Beth and Robinson, 1989). In particular, ST-EPR is well suited to the study of the rotational dynamics of integral membrane proteins (Thomas, 1985, 1986).

The analysis of ST-EPR spectra has been largely limited to the determination of parameters defined as the ratios of intensities in different regions of the spectra, followed by the comparison of these ratio parameters to those obtained from reference spectra either calculated assuming an isotropic rotational diffusion model (Beth et al., 1983) or obtained experimentally using model systems undergoing isotropic rotational diffusion such as spin-labeled hemoglobin in aqueous glycerol solutions (Thomas et al., 1976; Squier and Thomas, 1986). On the other hand, the rotational dynamics of many biological molecules, including integral membrane proteins, is expected to be highly anisotropic or restricted. Not suprisingly, the interpretation of ST-EPR data obtained from integral membrane proteins using model systems undergoing isotropic rotational diffusion can lead to order of magnitude uncertainties in the true characteristic rotation time (Beth et al., 1986; Beth and Robinson, 1989). A number of systems have been developed as models of anisotropic rotational diffusion (Gaffney, 1979; Delmelle et al., 1980; Fajer and Marsh, 1983). However, the application of results obtained from these specific model systems to integral membrane proteins, in general, has not been straightforward (Beth and Robinson, 1989).

Historically, the use of ratio parameters and isotropic model systems has been necessitated by the lack of computationally efficient algorithms for the calculation of ST-EPR spectra for anisotropic rotational diffusion models. Two basic approaches have been used to calculate ST-EPR spectra. Thomas and McConnell (1974) solved a system of diffusion-coupled Bloch equations, the transition-rate formalism, to calculate ST-EPR spectra for a nitroxide undergoing isotropic rotational diffusion assuming axial A- and g-tensors. Recently, this approach has been adapted to calculate ST-EPR spectra for a restricted anisotropic rotational diffusion model (Howard et al., 1993). Robinson and Dalton (1980) developed algorithms for solving the stochastic Liouville equation, expanding the nitroxide orientation distribution in terms of Wigner rotation matrix elements, to calculate ST-EPR spectra of a nitroxide undergoing anisotropic rotational diffusion. A similar approach has been used

Received for publication 1 February 1995 and in final form 30 June 1995.
Address reprint requests to Dr. Albert H. Beth, Department of Molecular Physiology and Biophysics, 727 Light Hall, Vanderbilt University, Nashville, TN 37232. Tel.: 615-322-4235; Fax: 615-322-7236; E-mail: beth@lhmbra.hh.vanderbilt.edu.

0006-3495/95/10/1409/15 $2.00

by Freed and co-workers to develop rapid algorithms for the simulation of linear EPR spectra of nitroxides for a variety of motional models (Freed, 1976; Schneider and Freed, 1989). The algorithms developed by Freed and co-workers have been used to perform detailed nonlinear least-squares analyses of the linear EPR lineshapes for biological systems such as spin-labeled lipids (Ge et al., 1994) and spin-labeled DNA oligomers (Hustedt et al., 1995).

It has been proposed that the dominant uniform rotational mode of a large integral membrane protein can be modeled as uniaxial rotational diffusion about the membrane normal axis (Saffman and Delbrück, 1975; Jähnig, 1986). However, to date, there has been relatively little rigorous experimental verification of this model (Cherry and Godfrey, 1981). These considerations have motivated the development of computationally efficient algorithms for the calculation of ST-EPR spectra for the uniaxial rotational diffusion model, which can be used to analyze experimental data obtained from ST-EPR studies of spin-labeled integral membrane proteins.

The transition-rate formalism has been used in this work to treat the uniaxial rotational diffusion of the nitroxide. When used for an isotropic rotational diffusion model, the transition-rate formalism requires either that the nitroxide A-and g-tensors are assumed to be axial or that a two-dimensional angular grid is used, greatly increasing the computation time. For uniaxial rotational diffusion, a one-dimensional angular grid may be used without the assumption of axial A- and g-tensors. The inclusion of nonaxial A- and g-tensor anisotropy is of critical importance for meaningful simulation of experimental data to determine the best-fit parameters for a particular rotational diffusion model, as is demonstrated by the analysis of ST-EPR spectra obtained for spin-labeled band 3 in intact erythrocytes presented here.

To model the spin dynamics, the Bloch equation approach is used. The alternative density matrix approach (Freed, 1976; Robinson and Dalton, 1980) does allow for rigorous treatment of the pseudosecular terms in the hyperfine interaction and also for the inclusion of nuclear spin relaxation (T_{1n}) effects that may be significant in ST-EPR. However, the inclusion of these effects significantly increases computation time (Thomas et al., 1976). The goal of this work was to develop accurate and computationally efficient algorithms for the calculation of ST-EPR for a nitroxide undergoing uniaxial rotational diffusion, which could then be incorporated into a nonlinear least-squares routine based on the Marquardt-Levenberg algorithm (Hustedt et al., 1993). Even with the large number of simulations required for iterative nonlinear least-squares analysis, the treatment of the spin dynamics in terms of Bloch equations is shown to be a reasonable approach. The effect of this and other approximations employed on the simulations will be discussed below.

In the following section, the equations for the calculation of ST-EPR spectra assuming the uniaxial rotational diffusion model are developed. Two different algorithms are presented. The first explicitly includes Zeeman overmodulation effects, whereas the second more rapid algorithm treats them approximately by using modified electron spin-lattice and spin-spin relaxation times. These algorithms are then used to perform nonlinear least-squares analysis of ST-EPR spectra of the anion exchange protein of the human erythrocyte membrane, known as band 3, which has been affinity spin-labeled with a newly developed dihydrostilbene disulfonate derivative, [^{15}N,$^{2}H_{13}$]-SL-H_2DADS-MAL (Wojcicki and Beth, 1993). The data are consistent with a model in which all copies of band 3 present in the intact erythrocytes undergo rotational diffusion about the membrane normal axis at a rate consistent with a band 3 dimer. These studies demonstrate the feasibility of detailed analysis of ST-EPR data in terms of relevant diffusion models and represent a significant advance in the analysis of ST-EPR data obtained for an integral membrane protein whose rotational dynamics have been the subject of considerable interest (Cherry et al., 1976; Nigg and Cherry, 1979; Tsuji et al., 1988; Matayoshi and Jovin, 1991; McPherson et al., 1992, 1993; Corbett and Golan, 1993).

THEORY

Algorithm I including Zeeman overmodulation effects

The approach outlined below closely follows that of McConnell and co-workers (McCalley et al., 1972; Thomas and McConnell, 1974). The equations are presented in some detail to make clear how they are adapted to calculate ST-EPR spectra assuming uniaxial rotational diffusion and to highlight where significant approximations have been made. We start with a set of Bloch equations describing the dynamics of the nitroxide spin magnetization in an orientation-dependent magnetic field that includes a term describing the rotational dynamics of the nitroxide spin-label.

$$\frac{d\vec{M}(\Omega(t), t)}{dt} = \vec{M}(\Omega(t), t) \times \gamma_e \vec{H}(\Omega(t), t) - \Gamma_R(\vec{M}(\Omega(t), t) - M_{eq}) - \Gamma_\Omega \vec{M}(\Omega(t), t) \quad (1)$$

The effective, orientation-dependent magnetic field in the rotating frame is taken to be

$$\gamma_e \vec{H}(\Omega(t), t) = [\gamma_e h_1]\hat{i} + [0]\hat{j} + [\Delta(\Omega(t), m_I) + \gamma_e h_m \cos(\omega_m t)]\hat{k}, \quad (2)$$

where

$$\Delta(\Omega(t), m_I) = \omega_o - g_{eff}(\Omega(t))\beta_e H_o + m_I A_{eff}(\Omega(t)) \quad (3)$$

and Ω is the complete set of angles describing the orientation of the nitroxide in the magnetic field, γ_e is the electron gyromagnetic ratio, β_e is the Bohr magneton, ω_0 is the applied microwave field frequency, h_1 is the microwave field amplitude, ω_m is the Zeeman modulation frequency,

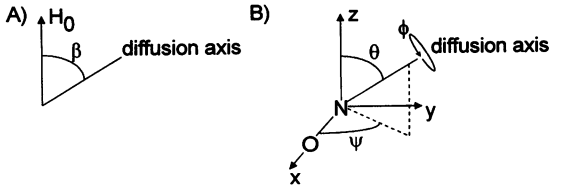

FIGURE 1 (*A*) The orientation of the uniaxial rotational diffusion axis with respect to the DC magnetic field of the spectrometer as determined by the angle β. (*B*) The orientation of the uniaxial rotational diffusion axis with respect to the nitroxide A-tensor as determined by the angles ψ, θ, and ϕ. The angles ψ and θ are assumed to be fixed. The third angle, ϕ, governs the rotation of the nitroxide about the uniaxial diffusion axis. The nitroxide A- and g-tensors are assumed to be coincident.

h_m is the Zeeman modulation field amplitude, and m_I is the nuclear spin state of the nitroxide nitrogen.

Consider a nitroxide spin-label undergoing uniaxial rotation diffusion about an axis oriented with respect to the DC magnetic field as determined by the angle β (see Fig. 1 *A*). It is assumed that there is an isotropic orientational distribution of diffusion axes relative to the DC magnetic field (the laboratory frame). The orientation of the nitroxide with respect to the diffusion axis is determined by the angles θ and ψ with a third angle, ϕ, governing the uniaxial rotational diffusion about this axis (see Fig. 1 *B*). It is assumed that the nitroxide adopts a unique labeling geometry with respect to the integral membrane protein and its rotational diffusion axis, and thus θ and ψ are fixed for all nitroxides in the sample. The values of A_{eff} and g_{eff} (Balasubramanian and Dalton, 1979) in Eq. 3 are determined by

$$A_{eff} = \sqrt{(A_{1,3})^2 + (A_{2,3})^2 + (A_{3,3})^2}$$
$$g_{eff} = g_{3,3}, \tag{4}$$

where $A_{i,j}$ and $g_{i,j}$ are elements of the coincident A- and g-tensors in the laboratory frame. The A-tensor in this frame is given by

$$A = R(O, \beta, O)R(\phi, \theta, \psi)A_dR^{-1}(\phi, \theta, \psi)R^{-1}(O, \beta, O), \tag{5}$$

where A_d is the diagonalized A-tensor in the nitroxide reference frame and the Rs are Euler angle rotation operators as defined by Edmonds (1957). A similar equation gives the elements of the g-tensor in the laboratory frame.

For uniaxial rotational Brownian diffusion, the diffusion operator is given by

$$\Gamma_\Omega = D_\parallel \frac{\partial^2}{\partial \phi^2}. \tag{6}$$

Choosing a discrete angular grid for ϕ,

$$\phi^n = \frac{2\pi(n-1)}{(N_\phi - 1)} \qquad n = 1, 2, \cdots, N_\phi \tag{7}$$

gives

$$\Gamma_\Omega \vec{M}^n = D_\parallel \lim_{N_\phi \to \infty} \frac{(\vec{M}^{n+1} - 2\vec{M}^n + \vec{M}^{n-1})}{\left(\frac{2\pi}{N_\phi - 1}\right)^2}$$
$$\approx \kappa \vec{M}^{n+1} - 2\kappa \vec{M}^n + \kappa \vec{M}^{n-1}, \tag{8}$$

where $\kappa = D_\parallel (N_\phi - 1)^2/4\pi^2$ and $\vec{M}^n$ is the magnetization vector corresponding to a particular value of ϕ^n.

Finally, spin relaxation is governed by

$$\Gamma_R \vec{M}^n = -\frac{1}{T_{2e}}(u^n \hat{i} + v^n \hat{j}) - \frac{1}{T_{1e}}(m_z^n - M_{eq}^n)\hat{k}, \tag{9}$$

where M_{eq}^n is the equilibrium magnetization at ϕ^n.

The equations of motion for the three components of the magnetization vectors are as follows:

$$\begin{aligned}
\dot{u}^n &= (-1/T_{2e} - 2\kappa)u^n \\
&\quad + (\Delta^n(m_I) + \gamma_e h_m \cos(\omega_m t))v^n + \kappa u^{n+1} + \kappa u^{n-1} \\
\dot{v}^n &= (-1/T_{2e} - 2\kappa)v^n - (\Delta^n(m_I) + \gamma_e h_m \cos(\omega_m t))u^n \\
&\quad + \gamma_e h_1 M_z^n + \kappa v^{n+1} + \kappa v^{n-1} \\
\dot{m}_z^n &= (-1/T_{1e})(M_z^n - M_{eq}^n) - 2\kappa M_z^n \\
&\quad - \gamma_e h_1 v^n + \kappa M_z^{n+1} + \kappa M_z^{n-1}.
\end{aligned} \tag{10}$$

Each of the three components is expanded as a Fourier series at harmonics of the Zeeman modulation frequency.

$$u^n = \sum_{k=-\infty}^{\infty} u_k^n e^{-ik\omega_m t} \qquad v^n = \sum_{k=-\infty}^{\infty} v_k^n e^{-ik\omega_m t}$$
$$m_z^n = \sum_{k=-\infty}^{\infty} M_{zk}^n e^{-ik\omega_m t} \tag{11}$$

Eq. 11 is substituted into Eq. 10, the resulting expressions integrated over one period of the modulation frequency to give a set of time-independent linear equations for the Fourier coefficients, and then the real and imaginary components of these coefficients are separated as follows:

$$u_k^n = U_k^n + iU_k^{n'} \qquad v_k^n = V_k^n + iV_k^{n'}$$
$$m_{zk}^n = M_{zk}^n + iM_{zk}^{n'}, \tag{12}$$

noting that the imaginary components of the $k = 0$ coefficients are zero and that

$$u_k^n = (u_{-k}^n)^* \qquad v_k^n = (v_{-k}^n)^* \qquad m_{zk}^n = (m_{z-k}^n)^*. \tag{13}$$

The complete set of steady-state equations to be solved can be written as follows:

$$W\vec{S} + \vec{Q} = O \tag{14}$$

where

$$W = \begin{pmatrix} W^1 - K & K & O & O & & \\ K & W^2 - 2K & K & O & & \\ O & K & W^3 - 2K & K & & \\ & & & \ddots & & \\ & & & K & W^{N_\phi - 1} - 2K & K \\ & & & & K & W^{N_\phi} - K \end{pmatrix} \tag{15}$$

with

$$\vec{S} = \begin{pmatrix} S^1 \\ S^2 \\ S^3 \\ \vdots \\ S^{N_\phi} \end{pmatrix} \qquad \vec{Q} = \begin{pmatrix} Q^1 \\ Q^2 \\ Q^3 \\ \vdots \\ Q^{N_\phi} \end{pmatrix} \tag{16}$$

and

$$K = \begin{pmatrix} \kappa & & & & & \\ & \kappa & & & & \\ & & \kappa & & & \\ & & & \kappa & & \\ & & & & \kappa & \\ & & & & & \cdot \end{pmatrix}. \tag{17}$$

The matrix W is block tridiagonal with the set of W^n along the diagonal describing the spin dynamics corresponding to a particular ϕ^n. Note that reflective boundary conditions have been used to describe the uniaxial rotational diffusion; i.e., there is a reflective boundary at $\phi^1 = 0$ and $\phi^{N_\phi} = 2\pi$. Although cyclic boundary conditions would be appropriate to describe uniaxial rotational diffusion, the use of reflective boundary conditions preserves the tridiagonal nature of W, which can be exploited to greatly increase the speed of the calculations. An understanding of the effect of this approximation on the calculated ST-EPR spectra can be gained from a consideration of the effect of the root-mean-squared (rms) amplitude of motion on ST-EPR spectra. In general, a relatively small rms amplitude of motion, between 10° and 90°, depending on the rate of rotational diffusion and θ (Howard et al., 1993), is required to achieve the full saturation transfer effect. Larger amplitudes of motion have no further effect on ST-EPR spectra. As a result, the contribution to the calculated ST-EPR spectra of those nitroxides not at orientations near $\phi = 0$ or $\phi = 2\pi$ should not be influenced by the presence of the reflective boundary. Those nitroxides near the boundary will, to some greater extent, be influenced by it. The effect of the assumption of reflective, rather than cyclic, boundary conditions will be considered further below via a direct comparison of calculated spectra (see Fig. 6 *D*).

The W^n matrices are likewise block tridiagonal with each W_k^n describing the dynamics of the magnetization corresponding to a particular ϕ^n at a particular modulation harmonic k. In practice the W^n are truncated to include only modulation harmonics up to $k = k_{max}$. Typically $k_{max} = 3$–5 is sufficient to give reasonable convergence of the signals at the second harmonic of the modulation frequency for a modulation amplitude of $h_m = 5$ Gauss.

$$W^n = \begin{pmatrix} W_0^n & C_{0,1} & 0 & 0 & 0 & \cdot \\ C_{1,0} & W_1^n & C_{1,2} & 0 & 0 & \cdot \\ 0 & C_{2,1} & W_2^n & C_{2,3} & 0 & \cdot \\ 0 & 0 & C_{3,2} & W_3^n & C_{3,4} & \cdot \\ 0 & 0 & 0 & C_{4,3} & W_4^n & \cdot \\ \cdot & \cdot & \cdot & \cdot & \cdot & \cdot \end{pmatrix} \tag{18}$$

with

$$S^n = \begin{pmatrix} S_0^n \\ S_1^n \\ S_2^n \\ S_3^n \\ S_4^n \\ \cdot \end{pmatrix} \qquad Q^n = \begin{pmatrix} Q_0^n \\ Q_1^n \\ Q_2^n \\ Q_3^n \\ Q_4^n \\ \cdot \end{pmatrix}. \tag{19}$$

Additional vectors and matrices are defined in the Appendix.

The steady-state solution to Eq. 14 can be efficiently obtained by using factorization methods appropriate for the case of a block tridiagonal matrix (Isaacson and Keller, 1966). This procedure requires the numerical inversion of N_ϕ W^n matrices whose dimensions are $3(2k_{max} + 1)$ by $3(2k_{max} + 1)$. If cyclic boundary conditions were used, the solution to Eq. 14 would require finding the numerical inverse of a single matrix, W, dimensioned $3N_\phi(2k_{max} + 1)$ by $3N_\phi(2k_{max} + 1)$.

The second harmonic out-of-phase absorption ST-EPR signal, $V_2'(\beta,m_I)$, corresponding to a particular orientation of the diffusion axis in the laboratory frame and a particular value of the nitroxide nitrogen nuclear spin state, is obtained from the sum

$$V_2'(\beta, m_I) = \sum_{n=1}^{N_\phi} V_2^{n'} \tag{20}$$

The total V_2' signal, corresponding to an isotropic distribution of diffusion axes, is obtained by performing the integral over β as a sum and by adding the contribution from the different values of the nitrogen nuclear spin state, m_I.

$$\begin{aligned} V_2' &= \sum_{m_I} \int_0^\pi V_2'(\beta, m_I)\sin(\beta)\, d\beta \\ &\approx \sum_{m_I} \sum_{j=1}^{N_\beta} V_2'(\beta^j, m_I)\sin(\beta^j) \end{aligned} \tag{21}$$

with

$$\beta^j = \frac{\pi(j - \tfrac{1}{2})}{N_\beta}. \tag{22}$$

The advantages of increased signal-to-noise ratio and increased spectral resolution obtained by using ^{15}N-enriched nitroxide spin-labels have been discussed extensively by Beth and Robinson (1989). It is also evident from Eq. 21 that calculations for a ^{15}N-enriched nitroxide will take only two-thirds as long as those for a natural abundance ^{14}N nitroxide. All of the calculated and experimental ST-EPR spectra presented here are for ^{15}N nitroxides. In many cases, the low cost and ready availability of ^{14}N nitroxide spin-labels may offset the advantages of using ^{15}N nitroxides and the extension of the work presented here to ^{14}N nitroxides is straightforward. Finally, to account for unresolved inhomogeneous broadening caused by hydrogen or deuterium nuclei not explicitly included in the spin Hamiltonian, the total V_2' signal given in Eq. 21 is convoluted with a Gaussian function of variable width, σ (Thomas et al., 1976).

Fig. 2 shows V_2' simulations as a function of k_{max}, the maximal number of harmonics over which the calculated signals are coupled. Although the required computation time increases by a factor of approximately five on going from $k_{max} = 2$ to $k_{max} = 5$, there is little change in the simulations for $k_{max} = 3$. The simulation of a 281-point, 70-Gauss-wide ST-EPR spectrum of a ^{15}N-enriched nitroxide for $k_{max} = 3$ requires approximately 3.5 h on a DEC 3000 400 workstation.

Figs. 3, 4, and 5 show V_2' simulations as a function of $\tau_\parallel = 1/6D_\parallel$, where $D_\parallel$ is the uniaxial rotational diffusion coefficient, and the angles θ and ψ, which determine the orientation of the nitroxide with respect to the diffusion axis (see Fig. 1 *B*). As expected, there is considerable sensitivity to $\tau_\parallel$ (Fig. 3) and θ (Fig. 4) at X-band microwave frequency ($\omega_0 \approx 10$ GHz). Given the value of θ used in Fig. 5, 30°, and the relatively small nonaxial character of the A-tensor, there is only slight sensitivity to ψ (Fig. 5) at X-band. The calculations shown in Figs. 3, 4, and 5 define the sensitivity of ST-EPR both to the rate of uniaxial rotational diffusion and the orientation of the nitroxide label with respect to the diffusion axis. This sensitivity to both diffusion rate and labeling geometry provides the motivation for the development of the nonlinear least-squares data analysis routines that are used below.

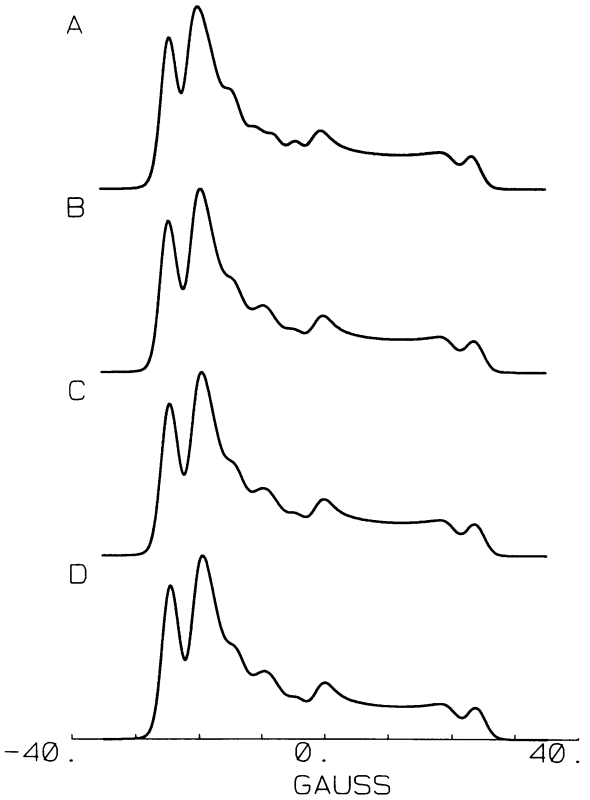

FIGURE 2 X-band V_2' ST-EPR spectra calculated using algorithm I for various values of $k_{max} = 2$ (*A*), 3 (*B*), 4 (*C*), and 5 (*D*) assuming $\tau_\parallel = 10$ μs, $\theta = 30°$, and $\psi = 60°$. Unless otherwise noted, calculations were performed using $\omega_0/2\pi = 9.76$ GHz, $h_1 = 0.2$ Gauss, $\omega_m/2\pi = 50$ kHz, $h_m = 5$ Gauss, $T_{1e} = 10$ μs, $T_{2e} = 150$ ns, $N_\beta = 128$, $N_\phi = 64$, and $k_{max} = 5$. All of the simulations shown in Figs. 2–7 have been convolved with a 1 Gauss Gaussian broadening function and the following A- and g-tensor elements were used: $g_{xx} = 2.008564$, $g_{yy} = 2.005917$, $g_{zz} = 2.002019$, $A_{xx} = 8.83$ Gauss, $A_{yy} = 8.41$ Gauss, and $A_{zz} = 45.77$ Gauss. These values are similar to those obtained from nonlinear least-squares analysis of the linear EPR spectrum of [^{15}N,$^2H_{13}$]-SL-H_2DADS-MAL-labeled erythrocytes at 37°C.

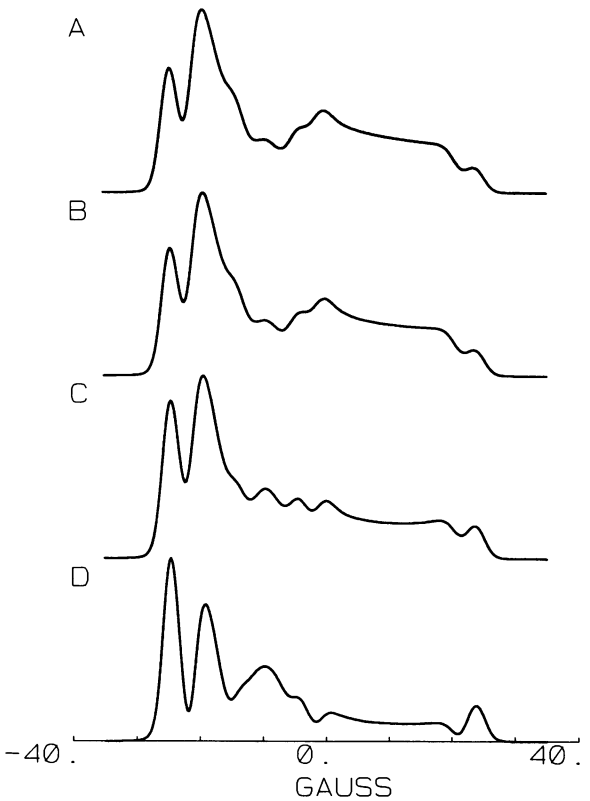

FIGURE 3 V_2' ST-EPR spectra calculated using algorithm I for various values of $\tau_\parallel = 1000$ (*A*), 100 (*B*), 10 (*C*), and 1 (*D*) μs assuming $\theta = 30°$ and $\psi = 0°$.

Algorithm II approximating Zeeman overmodulation effects

Although one of the important aspects of ST-EPR spectroscopy is the use of large Zeeman modulation fields, in the computational algorithm developed by Robinson and Dalton (1980), terms describing Zeeman overmodulation are dropped from the calculation resulting in a greatly reduced computation time. Instead, most of the Zeeman overmodulation effect can be approximated by using effective electron spin relaxation times, T_{1e}^{eff} and T_{2e}^{eff} (Robinson, 1983). In the equations developed above, Zeeman overmodulation effects are produced by the $C_{j-1,j}$ elements in W^n, which couple the signals at the jth harmonic back to those at the $j-1$th harmonic. Neglecting these back coupling terms, rearranging the matrix in Eq. 14, and calculating only those signals up to the second harmonic of the modulation frequency gives

$$W = \begin{pmatrix} W_0 & 0 & 0 \\ C_1 & W_1 & 0 \\ 0 & C_2 & W_2 \end{pmatrix} \qquad \vec{S} = \begin{pmatrix} S_0 \\ S_1 \\ S_2 \end{pmatrix} \qquad \vec{Q} = \begin{pmatrix} Q_0 \\ Q_1 \\ Q_2 \end{pmatrix} \tag{23}$$

with

$$W_k = \begin{pmatrix} W_k^1 - K & K & 0 & 0 & & & \\ K & W_k^2 - 2K & K & 0 & & & \\ 0 & K & W_k^3 - 2K & K & & & \\ & & & \ddots & & & \\ & & & & K & W_k^{N_\phi - 1} - 2K & K \\ & & & & & K & W_k^{N_\phi} - K \end{pmatrix} \tag{24}$$

$$S_k = \begin{pmatrix} S_k^1 \\ S_k^2 \\ S_k^3 \\ \vdots \\ S_k^{N_\phi} \end{pmatrix} \qquad Q_k = \begin{pmatrix} Q_k^1 \\ Q_k^2 \\ Q_k^3 \\ \vdots \\ Q_k^{N_\phi} \end{pmatrix}$$

and

$$C_1 = \begin{pmatrix} C_{1,0} & & & & \\ & C_{1,0} & & & \\ & & C_{1,0} & & \\ & & & \ddots & \\ & & & & C_{1,0} \end{pmatrix} \qquad C_2 = \begin{pmatrix} C_{2,1} & & & & \\ & C_{2,1} & & & \\ & & C_{2,1} & & \\ & & & \ddots & \\ & & & & C_{2,1} \end{pmatrix}. \tag{25}$$

In this case, the second harmonic ST-EPR signals can be obtained as follows:

$$S_0 = (W_0)^{-1} Q_0 \qquad S_1 = (W_1)^{-1}(-C_1 S_0 - Q_1) \qquad S_2 = (W_2)^{-1}(-C_2 S_1 - Q_2) \tag{26}$$

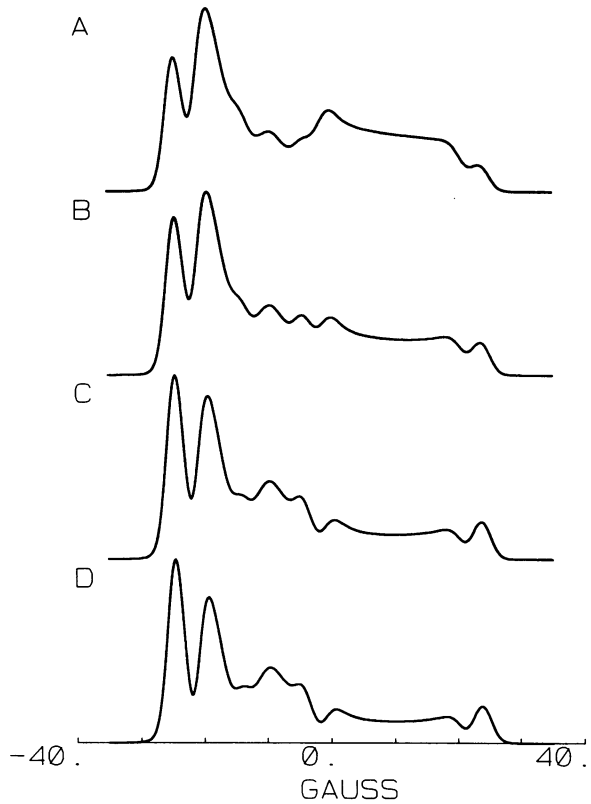

FIGURE 4 V_2' ST-EPR spectra calculated using algorithm I for various values of $\theta = 0°$ (A), 30° (B), 60° (C), and 90° (D) assuming $\tau_\parallel = 10\ \mu s$ and $\psi = 0°$.

Solving Eq. 26 requires taking the numerical inverse of N_ϕ matrices (W_0^n) dimensioned 3 by 3 and $2N_\phi$ matrices (W_1^n and W_2^n) dimensioned 6 by 6.

Figs. 6 and 7 show V_2' simulations (solid lines) calculated as a function of $\tau_\parallel$ and θ, neglecting Zeeman overmodulation terms and using effective electron spin relaxation times, T_{1e}^{eff} and T_{2e}^{eff}. For the calculations shown, the values of T_{1e}^{eff} and T_{2e}^{eff} were those that optimized the agreement of the calculation in Fig. 6 C (algorithm II) with that in Fig. 3 C (algorithm I) as determined by a nonlinear least-squares analysis. Qualitatively, the trends seen in Figs. 6 and 7 follow those seen in the corresponding Figs. 3 and 4.

Overlaid on the uniaxial rotational diffusion simulations in Figs. 6 and 7 are simulations (dashed lines) obtained by using the eigenfunction expansion approach developed by Robinson and Dalton (1980), demonstrating the reasonable agreement between the two approaches. The Robinson and Dalton algorithm performs calculations assuming an axial rotational diffusion model and includes a nitrogen nuclear spin relaxation time, T_{1n}. To compare with the uniaxial calculations approach developed here, the Robinson and Dalton algorithm was used with $\tau_{perp} = 10$ ms and $T_{1n} = 1$ ms. Both of these times were sufficiently long to have no effect on the calculated spectrum. Other differences in the approximations used in these two approaches will be discussed below.

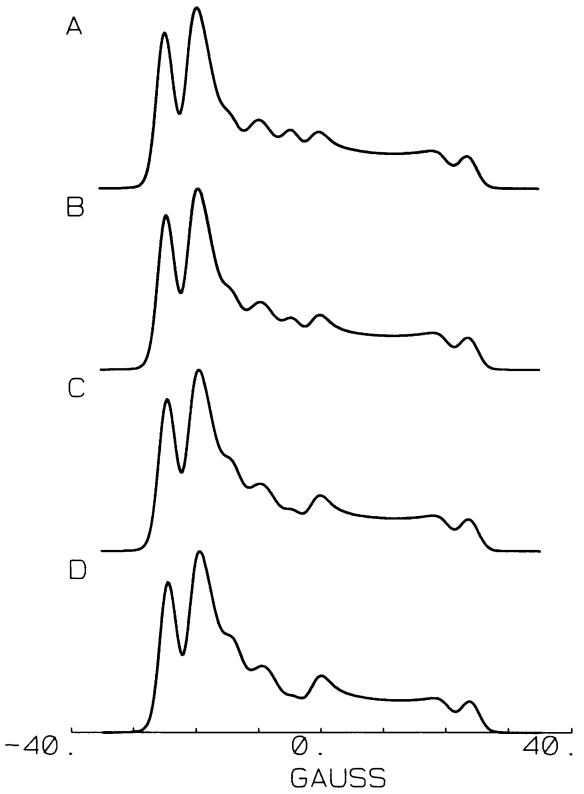

FIGURE 5 V_2' ST-EPR spectra calculated using algorithm I for various values of $\psi = 0°$ (*A*), 30° (*B*), 60° (*C*), and 90° (*D*) assuming $\tau_{\|} = 10$ μs and $\theta = 30°$.

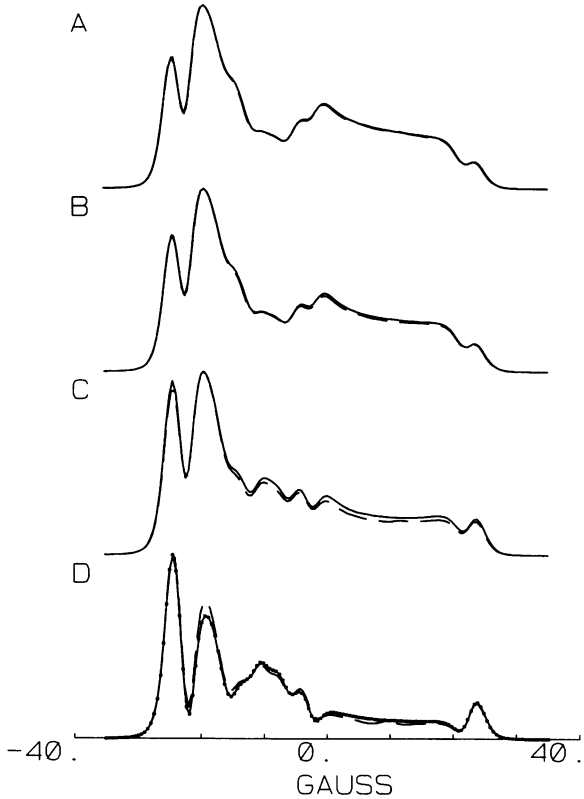

FIGURE 6 V_2' ST-EPR spectra calculated using algorithm II (solid lines) for various values of $\tau_{\|} = 1000$ (*A*), 100 (*B*), 10 (*C*), and 1 (*D*) μs assuming $\theta = 30°$, $\psi = 0°$, $T_{1e}^{eff} = 13$ μs, $T_{2e}^{eff} = 42$ ns, and $N_\beta = N_\phi = 64$. Overlaid dashed lines were calculated using the routine developed by Robinson and Dalton (1980) for the same values of $\tau_{\|}$, θ, T_{1e}^{eff}, and T_{2e}^{eff}, assuming highly anisotropic rotational diffusion with $\tau_{perp} = 10$ ms and $T_{1n} = 1$ ms. The overlaid dotted line in *D* was calculated assuming cyclic, rather than reflective, boundary conditions ($N_\beta = 64$; $N_\phi = 32$).

Overlaid on the simulations shown in Fig. 6 *D* is a third simulation (dotted line) calculated by using the algorithm II as outlined above but assuming cyclic rather than reflective boundary conditions. In this case, the matrices W_k (Eq. 4) are replaced by

$$W_k = \begin{pmatrix} W_k^1 - 2K & K & 0 & 0 & & & K \\ K & W_k^2 - 2K & K & 0 & & & \\ 0 & K & W_k^3 - 2K & K & & & \\ & & & \ddots & & & \\ & & & & K & W_k^{N_\phi - 1} - 2K & K \\ K & & & & & K & W_k^{N_\phi} - 2K \end{pmatrix} \quad (27)$$

and the solution to Eq. 26 requires finding the numerical inverse of a single matrix (W_0) dimensioned $3N_\phi$ by $3N_\phi$ and two matrices (W_1 and W_2) dimensioned $6N_\phi$ by $6N_\phi$. Under reflective boundary conditions, the required computation time is linear in N_ϕ. Under cyclic boundary conditions, computation time goes as N_ϕ^3. It is important to note that the calcutions assuming reflective boundary condition (solid line) and cyclic boundary conditions (dotted line) in Fig. 6 *D* are virtually identical. In this case, the use of reflective boundary conditions greatly reduces computation time without any significant effect on the calculated spectra. Moreover, the effect of the change in boundary conditions is expected to be decreased as $\tau_{\|}$ increases.

Algorithm I and the eigenfunction expansion approach of Robinson and Dalton (1980) require approximately the same computation time. Although the eigenfunction expansion approach includes the pseudosecular terms of the hyperfine interaction, optimizing the transition-rate formalism for the uniaxial rotational diffusion model allows for explicit treatment of Zeeman overmodulation effects. The inclusion of Zeeman overmodulation terms allows spectra to be analyzed in terms of true spin-relaxation times, T_{1e} and T_{2e}, rather than effective spin relaxation times (Robinson, 1983). Using the transition-rate formalism and neglecting the nonlinear Zeeman modulation effects reduces computation time by approximately a factor of 20 relative to the eigenfunction expansion approach and algorithm I. An important aspect of the reduction in computation times obtained is the use of reflective boundary conditions.

MATERIALS AND METHODS

The synthesis of the spin-labeled dihydrostilbene disulfonate derivative, [^{15}N,^{2}H$_{13}$]-SL-H$_2$DADS-MAL (Fig. 8), and its use as a band 3 affinity spin-label in intact erythrocytes will be described in detail elsewhere (D. J.

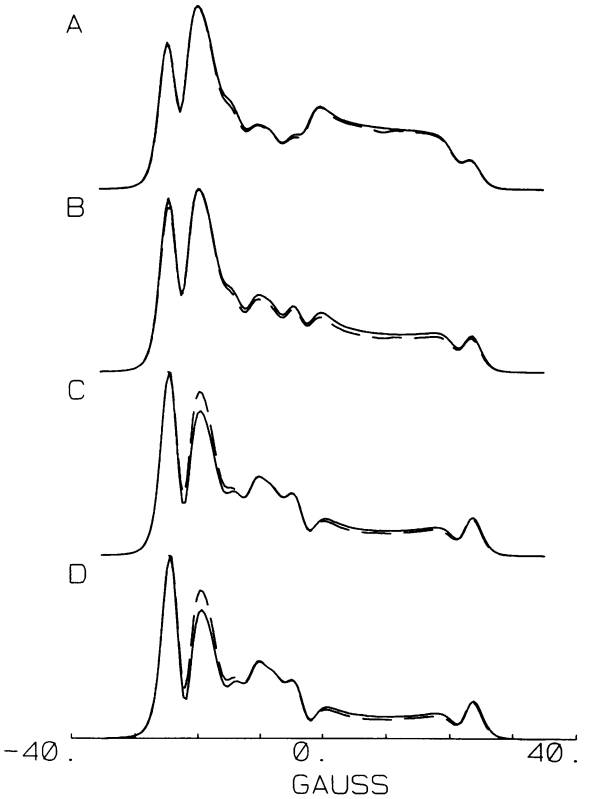

FIGURE 7 V_2' ST-EPR spectra calculated using algorithm II (solid lines) for various values of θ = 0° (*A*), 30° (*B*), 60° (*C*), and 90° (*D*) assuming $\tau_{\|}$ = 10 μs, ψ = 0°, T_{1e}^{eff} = 13 μs, T_{2e}^{eff} = 42 ns, and $N_\beta = N_\phi$ = 64. Overlaid dashed lines were calculated using the routine developed by Robinson and Dalton (1980), assuming highly anisotropic rotational diffusion with τ_{perp} = 10 ms and T_{1n} = 1 ms.

Scothorn, W. E. Wojcicki, E. J. Hustedt, A. H. Beth, and C. E. Cobb, manuscript in preparation) some preliminary data have appeared in abstract form (Wojcicki and Beth, 1993). The labeling procedure employed was similar to those reported for other band 3 affinity spin-labels (e.g., Beth et al., 1986). Heparinized whole blood, freshly drawn from normal adult donors, was washed three times with 113 mM sodium citrate buffer, pH 7.4, to remove the plasma and buffy coat. Erythrocytes were then incubated with 28 μM [^{15}N,^{2}H$_{13}$]-SL-H$_2$DADS-MAL in buffer for 60 min on ice and then incubated for 30 min on ice after addition of 10 vol of 0.2% (w/v) bovine serum albumin (fraction V, Sigma Chemical Co., St. Louis, MO) in buffer. The cells were then washed (centrifuged, separated from the supernatant, and resuspended in buffer) once with 0.2% bovine serum albumin and then twice with buffer. All EPR spectra were collected from samples of loosely packed intact human erythrocytes in 113 mM sodium citrate buffer, pH 7.4, contained in 50-μl disposable micropipettes (Corning Science Products, Corning, NY) at 37°C. Spectra were collected with a Bruker (Billerica, MA) ESP-300 spectrometer equipped with an ER 4103

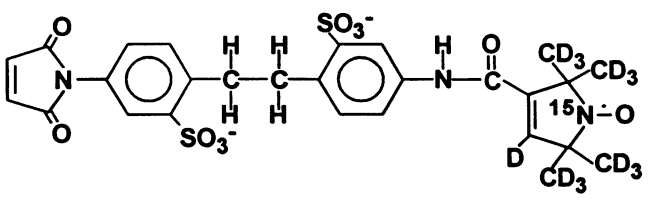

FIGURE 8 The chemical structure of [^{15}N,^{2}H$_{13}$]-SL-H$_2$DADS-MAL.

(TM$_{110}$) cavity. Temperature was maintained by blowing N_2 gas, equilibrated at the appropriate temperature, through the front optical port of the cavity. The linear EPR spectrum of [^{15}N,^{2}H$_{13}$]-SL-H$_2$DADS-MAL-labeled band 3 in intact erythrocytes at 37°C in buffer was measured and analyzed, as previously described (Hustedt et al., 1993), to determine the principal elements of the nitroxide A- and g-tensors, which were then used to analyze the ST-EPR spectra. The ST-EPR spectra were obtained by using a 0.2-Gauss microwave field, 5-Gauss Zeeman modulation field, and Zeeman modulation frequencies of 100, 50, and 25 kHz. Microwave and Zeeman modulation field amplitudes were calibrated using peroxyl amine disulfonate (Aldrich Chemical Co., Milwaukee, WI) as described previously (Beth et al., 1983). The algorithms described above for calculating ST-EPR spectra assuming the uniaxial rotational diffusion model have been incorporated into a nonlinear least-squares analysis routine, based on the Marquardt -Levenberg algorithm, which has been described in detail elsewhere (Hustedt et al., 1993). Analysis of ST-EPR spectra in terms of an isotropic rotational diffusion model has also been previously described (Hustedt et al., 1993). All calculations were performed on a DEC 3000 400 workstation (Digital Equipment Corp., Maynard, MA).

RESULTS

The V_2' ST-EPR spectra of [^{15}N,^{2}H$_{13}$]-SL-H$_2$DADS-MAL-labeled band 3 in intact erythrocytes at 37°C obtained by using 100-, 50-, and 25-kHz Zeeman modulation frequencies are shown in Fig. 9. Overlaid on the data in Fig. 9 are fits obtained by a simultaneous nonlinear least-squares analysis of the three data sets using algorithm II, neglecting Zeeman overmodulation terms. In addition to the results presented in Fig. 9, six separate analyses were performed as outlined in Table 1. Initial values of $\tau_{\|} = 1/6D_{\|}$ = 50 or 1 μs and $\theta = \psi$ = 10, 45, or 90° were used to start the Marquardt-Levenberg algorithm. All six analyses gave essentially the same results, suggesting the lack of local minima in the χ^2 surface.

Recent time-resolved optical anisotropy studies of eosin-labeled band 3 by Matayoshi and Jovin (1991) and McPherson et al. (1992) have revealed components of the anisotropy decays in the 10 to 30 μs range. For the uniaxial rotational diffusion model these decay times correspond to $1/D_{\|}$ or $1/4D_{\|}$ (depending on the orientation of the absorption and emission dipoles of eosin to the diffusion axis) and are in reasonable agreement with the value of $\tau_{\|} = 1/6D_{\|}$ obtained here. Additional longer decay components are also observed in optical anisotropy experiments and are typically ascribed to a population of band 3 whose rotational dynamics is restricted by interactions involving the cytoplasmic domain or to a population of band 3 oligomers larger than a dimer. The use of multiple Zeeman modulation frequencies is intended to detect multiple populations of band 3 with different rotational properties, if they are present (Beth and Robinson, 1989). No evidence is found in the ST-EPR results presented here of multiple populations of band 3 with different rotational characteristics. An attempt to analyze the ST-EPR data in Fig. 9 in terms of two populations of band 3 with different characteristic values of $\tau_{\|}$ (starting the nonlinear least-squares analysis with $\tau_{\|}$ = 10 and 100 μs) produced a result in which the two characteristic values of $\tau_{\|}$ were essentially equal ($\tau_{\|}$ = 13.5 and 14.3 μs) with no improvement in the global χ^2.

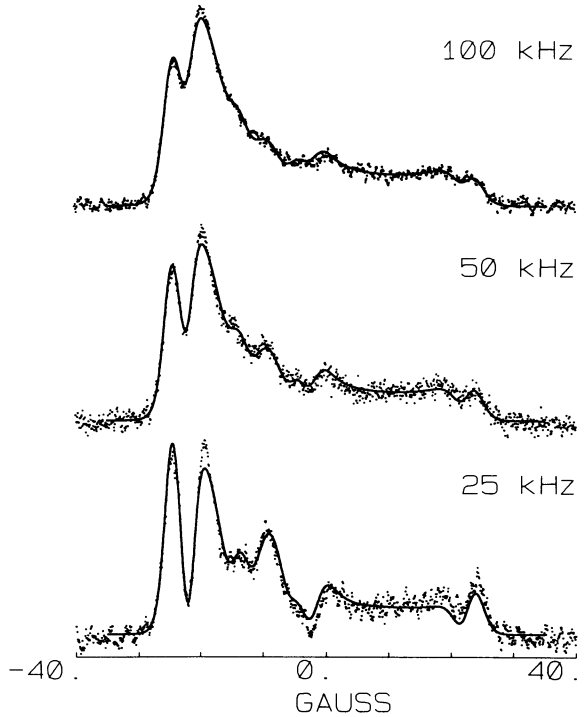

FIGURE 9 V_2' ST-EPR spectra (dots) of [^{15}N,^{2}H$_{13}$]-SL-H$_2$DADS-MAL-labeled band 3 in intact erythrocytes at 37°C obtained for Zeeman modulation frequencies of $\omega_m/2\pi$ = 100 (*A*), 50 (*B*), and 25 (*C*) kHz. Overlaid fits (solid lines) were obtained from a simultaneous analysis of the three data sets using the more rapid algorithm II, which neglects terms describing Zeeman overmodulation effects to give $\tau_\parallel$ = 15 μs, θ = 37°, ψ = 61°, and T_{1e}^{eff} = 1 μs, T_{2e}^{eff} = 56 ns, and σ = 1.4 Gauss (*A*); T_{1e}^{eff} = 5 μs, T_{2e}^{eff} = 69 ns, and σ = 1.3 Gauss (*B*); and T_{1e}^{eff} = 9 μs, T_{2e}^{eff} = 148 ns, and σ = 1.3 Gauss (*C*). Total χ^2 = 1.68. The nitroxide A- and g-tensors were obtained from a nonlinear least-squares analysis of a linear EPR spectrum of the same sample (data and fit not shown): g_{xx} = 2.00854, g_{yy} = 2.00589, g_{zz} = 2.00207, A_{xx} = 8.2 Gauss, A_{yy} = 7.9 Gauss, and A_{zz} = 45.8 Gauss. Total χ^2 = 2.20. Calculations were performed using $N_\beta = N_\phi$ = 96.

The same data are repeated in Fig. 10, where the overlaid nonlinear least-squares fits were calculated using algorithm I, which explicitly includes the Zeeman overmodulation effects. The results of the two approaches, neglecting (Fig. 9) and including (Fig. 10) Zeeman overmodulation terms are in reasonable agreement. However, there is a decrease in the value of $\tau_\parallel$ obtained when the Zeeman overmodulation effects are included. The fitting parameters optimized in the least-squares analysis of these spectra were $\tau_\parallel = 1/6D_\parallel$ = 8 μs, which defines the rate of uniaxial rotational diffusion; θ = 34° and ψ = 66°, which determine the orientation of the nitroxide with respect to the diffusion axis; T_{1e} = 11 μs and T_{2e} = 270 ns, which determine the rates of electron spin-lattice and spin-spin relaxation; and the set of σ values, which are used to account for broadening caused by unresolved electron-deuterium couplings. The value of σ was allowed to vary with ω_m; however all three spectra were fit with $\sigma \approx 1$ Gauss.

An important prediction of the uniaxial rotational diffusion model is that the rotation axis is the membrane normal vector. The orientation of the nitroxide with respect to the diffusion axis, given by θ and ψ, is essentially identical to the orientation of the nitroxide with respect to the membrane normal as determined from linear EPR studies of [^{15}N,^{2}H$_{13}$]-SL-H$_2$DADS-MAL-labeled band 3 in flow-oriented erythrocytes. Details of these orientation studies will appear elsewhere (Hustedt and Beth, manuscript in

TABLE 1 Results of six non-linear least-squares analyses of V_2' ST-EPR spectra of [^{15}N,^{2}H$_{13}$]-SL-H$_2$DADS-MAL-labeled band 3 in intact erythrocytes at 37°C obtained for Zeeman modulation frequencies of 100, 50, and 25 kHz

Initial values			Optimized values			
$\tau_\parallel$	ψ	θ	$\tau_\parallel$	ψ	θ	Global χ^2
50 μs	10°	10°	14.7 μs	60.9°	36.9°	1.681
1 μs	10°	10°	14.7 μs	61.0°	36.9°	1.681
50 μs	45°	45°	14.7 μs	60.7°	36.9°	1.681
1 μs	45°	45°	15.4 μs	61.7°	37.6°	1.680
50 μs	90°	90°	14.4 μs	61.3°	36.9°	1.682
1 μs	90°	90°	15.2 μs	61.5°	38.0°	1.682

Each analysis required between 9 and 15 iterations of the Marquardt-Levenberg algorithm and approximately 2 to 3 days of computation time. In all cases, initial values of T_{1e}^{eff} = 10 μs, T_{2e}^{eff} = 50 ns, and σ = 1 Gauss were used and the best-fit values of T_{1e}^{eff}, T_{2e}^{eff}, and σ obtained were similar to those listed for Fig. 9.

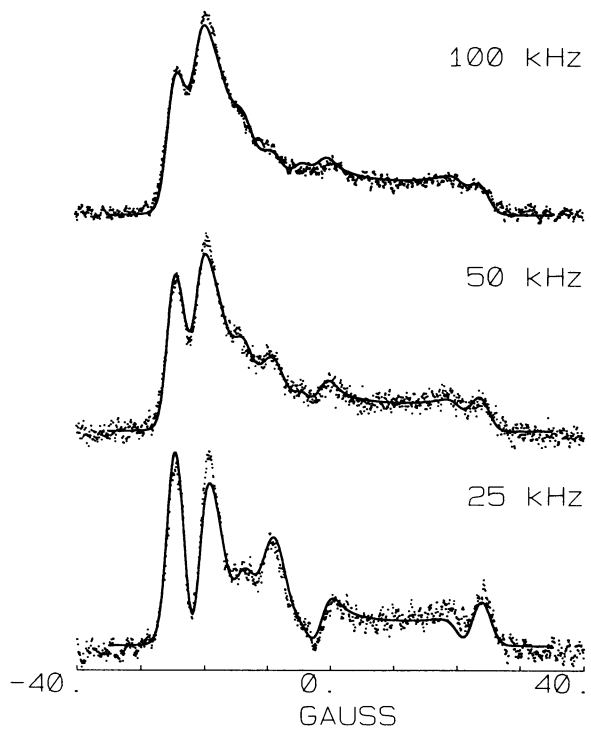

FIGURE 10. Same data as Fig. 9. Overlaid fits were obtained from a simultaneous nonlinear least-squares analysis of the three data sets using algorithm I to give $\tau_\parallel$ = 8 μs, θ = 34°, ψ = 66°, T_{1e} = 11 μs, and T_{2e} = 270 ns and Gaussian broadening parameters of σ = 1.0 Gauss (*A*), 1.0 Gauss (*B*), and 1.0 Gauss (*C*). Calculations were performed using $N_\beta = N_\phi$ = 96, and k_{max} = 4. Initial values of τ, θ, and ψ were obtained from the nonlinear least-squares analysis of the same data using algorithm II (see Fig. 9).

preparation); a preliminary report has appeared in abstract form (Hustedt and Beth, 1994a,b).

According to the theoretical predictions of Saffman and Delbrück (1975), the expected rate of uniaxial rotational diffusion for an integral membrane protein, modeled as a circular cylinder, is given by

$$D_{\parallel} = \frac{kT}{4\pi\eta r^2 h}, \tag{28}$$

where η is the membrane viscosity, r is the radius of the cylinder, and h is the height of the lipid bilayer. Recently, electron microscopy images of the transmembrane domain of band 3 reconstituted with lipids into two-dimensional crystals have been obtained, which provide reasonable estimates of the size of the integral membrane domain (Wang et al., 1993, 1994). The band 3 dimer forms elongated structures in which the largest dimension of the transmembrane domain of the band dimer is approximately 110 Å and the cross-sectional area of the dimer (in the plane parallel to the lipid bilayer) is approximately 3000 Å^2 (Wang et al., 1994). From the largest dimension an upper limit of $r = 55$ Å is obtained. On the other hand, a circular cylinder with the equivalent cross-sectional area would have a radius of $r = 31$ Å. A reasonable estimate of the lipid bilayer height in the erythrocyte membrane (headgroup to headgroup) is 48 Å (McCaughan and Krimm, 1980). On the other hand, Wang et al. (1994) estimate the thickness of the transmembrane domain of band 3 to be 40 Å. Using these values and the value of $\tau_{\parallel} = 1/6D_{\parallel}$ of 8 μs obtained at 37°C, the range of estimates for the effective membrane viscosity obtained from Eq. 28 is 1.1–4.3 poise. These values are within the range of ~0.5–4 poise, which has been reported for model and biological membranes using a variety of experimental techniques (van der Meer, 1993). Therefore, to the extent that the various parameters in Eq. 28 have been defined by other experimental methods, the characteristic rotation time of 8 μs is consistent with the uniform rotational motion of a band 3 dimer in the membrane.

The fits shown in Fig. 9 using the more approximate algorithm II are better ($\chi^2 = 1.68$) than those shown in Fig. 10 ($\chi^2 = 2.20$) obtained using algorithm I. This apparent improvement in the fits using the more approximate algorithm is because of the difference in how electron spin relaxation is treated in the two algorithms. For algorithm I, T_{1e} and T_{2e} are the true intrinsic electron spin-lattice and electron spin-spin relaxation times. For algorithm II, T_{1e}^{eff} and T_{2e}^{eff} are effective relaxation times modified to account for the neglect of Zeeman overmodulation terms and are Zeeman modulation frequency dependent (Robinson, 1983). Thus, for the fits shown in Fig. 10, the values of $\tau_{\parallel}$, ψ, θ, T_{1e}, and T_{2e} are all required to be the same for the three data sets, i.e., linked in the language of global analysis (Beechem et al., 1991). The Gaussian broadening parameters, σ, are not linked, but the best-fit value, $\sigma \approx 1$ Gauss, is the same for all three spectra. In Fig. 9, only $\tau_{\parallel}$, ψ, and θ are linked. For direct comparison with the results using algorithm I, analyses have been performed using algorithm II in which the values of T_{1e}^{eff} and T_{2e}^{eff} are linked. These analyses have consistently given a total χ^2 value greater than 5. When this direct comparison is made, algorithm I, which explicitly includes the Zeeman overmodulation terms, does give a substantially better fit ($\chi^2 = 2.20$).

The same data are repeated again in Fig. 11, in which the overlaid fits were calculated assuming an isotropic rotational diffusion model and using an algorithm that neglects Zeeman overmodulation effects (Robinson and Dalton, 1980). Reasonable fits are also obtained for the isotropic rotational diffusion model, using an isotropic rotational correlation time of 115 μs.

The ability of ST-EPR spectroscopy to distinguish between isotropic and uniaxial rotational diffusion models is in large part determined by the orientation of the nitroxide relative to the uniaxial rotational diffusion axis. It is expected that the differences between the two models will be greatest for $\theta = 90°$. The simulations shown in Fig. 9, for uniaxial rotational diffusion ($\tau_{\parallel} = 15$ μs and $\theta = 37°$), and Fig. 11, for isotropic rotational diffusion ($\tau_{iso} = 115$ μs), were both performed using algorithms that drop Zeeman overmodulation terms. The simulations themselves are nearly indistinguishable and the differences between them are within the accuracy of the various approximations employed.

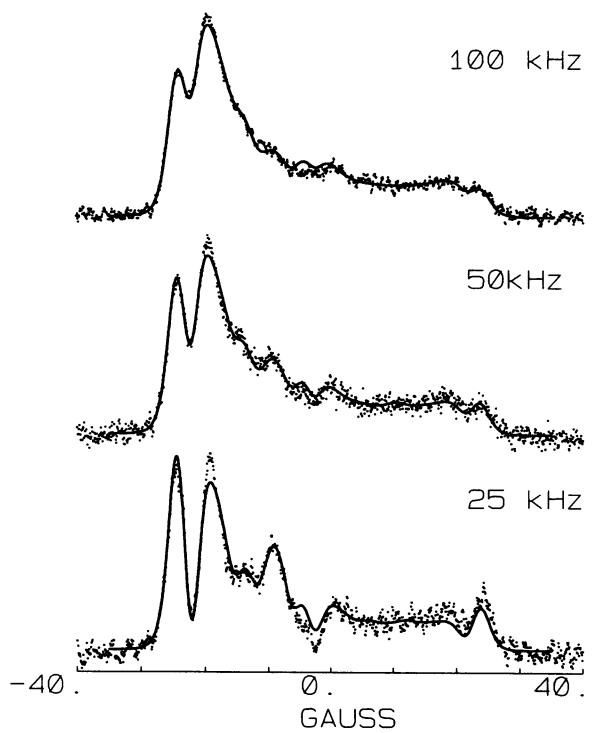

FIGURE 11. Same data as Fig. 9. Overlaid fits (solid lines) were obtained from a simultaneous analysis of the three data sets using an isotropic rotational diffusion model (Robinson and Dalton, 1980; Hustedt et al., 1993) using an algorithm that neglects terms describing Zeeman overmodulation effects to give $\tau_{iso} = 115$ μs and $T_{1e}^{eff} = 2$ μs, $T_{2e}^{eff} = 41$ ns, and $\sigma = 1.3$ Gauss (*A*); $T_{1e}^{eff} = 10$ μs, $T_{2e}^{eff} = 47$ ns, and $\sigma = 1.1$ Gauss (*B*); $T_{1e}^{eff} = 22$ μs, $T_{2e}^{eff} = 84$ ns, and $\sigma = 1.1$ Gauss (*C*). Total $\chi^2 = 1.79$.

DISCUSSION

ST-EPR simulations for the uniaxial rotational diffusion model

The significant approximations used in algorithm I are the use of reflective boundary conditions, the neglect of the intrinisic ^{15}N nuclear spin-lattice relaxation time, T_{1n}, and the treatment of the pseudosecular terms of the high-field spin Hamiltonian

$$\hat{H}(\Omega(t)) = g_{zz}\beta_e H S_z - \omega_n I_z + A_{xz}(\Omega(t))I_x S_z + A_{yz}(\Omega(t))I_y S_z + A_{zz}(\Omega(t))I_z S_z \quad (29)$$

in terms of a single, effective secular term

$$\hat{H}(\Omega(t)) = g_{zz}\beta_e H S_z - \omega_n I_z + m_I A_{eff}(\Omega(t))S_z, \quad (30)$$

which is obtained from a diagonalization of the Hamiltonian of Eq. 29 by a rotation operator of the form $e^{i\omega I_z}$. The rotation angle, ω, required to diagonalize the Hamiltonian in Eq. 29 is a function of the orientation, Ω, of the nitroxide in the magnetic field. The use of Eq. 29 requires the treatment of the spin dynamics in terms of a density matrix approach, whereas Eq. 30 allows the spin dynamics to be treated in terms of the Bloch equations. For the calculation of linear EPR spectra, the latter approach is valid in the rigid limit (Balasubramanian and Dalton, 1979); however, it clearly gives incorrect results in the fast motion limit, $\tau \leq 5$ ns (McCalley et al., 1972). For the calculation of ST-EPR spectra, this approximation reduces the size of the W_k^n matrices from 6 by 6 to 3 by 3 for $k = 0$ and from 15 by 15 to 6 by 6 for $k \geq 1$. As a result there is a dramatic reduction in computation time. The effect on the accuracy of the ST-EPR simulations of using the Hamiltonian of Eq. 30, rather than Eq. 29, will be addressed below in the context of algorithm II.

In the case of algorithm II, the terms describing the effect of Zeeman overmodulation are dropped from the calculation. The calculations shown in Figs. 6 and 7 show that, in qualitative agreement with Robinson (1983), much of the overmodulation effect can be accounted for by using effective electron spin relaxation times, T_{1e}^{eff} and T_{2e}^{eff}. Overlaid on the uniaxial rotational diffusion simulations in Figs. 6 and 7 are simulations (dashed lines) obtained by using the program originally developed by Robinson and Dalton (1980), using an eigenfunction expansion approach, to calculate ST-EPR spectra assuming anisotropic rotational diffusion. The Robinson and Dalton approach likewise drops the nonlinear Zeeman modulation terms; however, it does explicitly include T_{1n} and the pseudosecular terms of the spin Hamiltonian. There is reasonable agreement between the two approaches, particularly for large $\tau_\parallel$ and small θ, suggesting that the neglect of T_{1n} and the approximate treatment of the pseudosecular terms is more valid for slower effective motional rates. The most significant disagreements between the two calculations are in the height of the L″ region of the spectra (the second peak from the left). A single calculation (Fig. 6D, dotted line) performed using algorithm II and cyclic boundary conditions suggests that the use of reflective boundary conditions does not produce significant errors. As a result, it can be concluded that the discrepancy between algorithm II (solid line) and the Robinson and Dalton algorithm (dashed lines) evident in Figs. 6 and 7 are caused solely by the use of the Hamiltonian in Eq. 30 versus that of Eq. 29. The use of the simpler Hamiltonian and the transition-rate formalism (with reflective boundary conditions) to treat the uniaxial rotational diffusion results in over an order of magnitude decrease in computation time for algorithm II versus the Robinson and Dalton algorithm.

The reasonable agreement between calculations performed using algorithm II and those performed using algorithm I or the Robinson and Dalton algorithm demonstrates that algorithm II is useful for performing initial analyses of ST-EPR data and for exploring χ^2 surfaces. Algorithm I allows a more accurate treatment of Zeeman overmodulation effects, whereas the Robinson and Dalton algorithm allows a more accurate treatment of the electron-nuclear hyperfine interaction. Both of these more accurate approaches can be used to refine preliminary fits obtained using algorithm II. The Robinson and Dalton (1980) approach also allows for testing of isotropic and axial rotational diffusion models. Finally, it should be emphasized that the intrinsic T_{1e} and T_{2e} values obtained from algorithm I can be directly compared with values obtained from time-domain saturation recovery and electron spin-echo experiments. Together, these three algorithms provide a reasonable approach to the nonlinear least-squares analysis of ST-EPR spectra as has been demonstrated here for data obtained from [^{15}N,$^{2}H_{13}$]-SL-H_2DADS-MAL-labeled band 3 in intact erythrocytes.

Band 3

ST-EPR spectroscopy has been widely used to study the rotational dynamics of large integral membrane proteins and uniaxial rotational diffusion is frequently invoked as a model to describe the global rotational diffusion of such proteins. To date, however, the complexity of the required calculations has prevented the rigorous analysis of ST-EPR data specifically in terms of the uniaxial rotational diffusion model. Transient absorption anisotropy and time-resolved phosphorescence emission anisotropy are alternative techniques for studying rotational dynamics on the microsecond to millisecond time scale. For these techniques, data analysis is much simpler, requiring the fitting of data to exponential or multiexponential decays. However, as discussed by Matayoshi and Jovin (1991), the interpretation of the multiexponential anisotropy decay data is often ambiguous. As a result, optical-based techniques have provided limited evidence of the validity of the uniaxial rotational diffusion model (see, for example, studies of bacteriorhodopsin by Cherry and Godfrey, 1981).

The rotational diffusion of band 3, the anion exchange protein of the human erythrocyte membrane, has been extensively studied, primarily by the detection of the transient absorption anisotropy or time-resolved phosphorescence emission anisotropy of eosin-labeled band 3 in erythrocyte ghost membranes (Cherry et al., 1976; Nigg and Cherry, 1979; Tsuji et al., 1988; Matayoshi and Jovin, 1991; McPherson et al., 1992, 1993; Corbett and Golan, 1993). The motivation behind these studies is the expected sensitivity of rotational diffusion to the oligomeric state of band 3 and to the mechanical properties of various other protein-protein interactions involving the cytoplasmic domain of band 3. ST-EPR offers an alternative technique for the measurement of rotational diffusion on the microsecond to millisecond time scale and a number of different band 3 affinity spin-labels have been developed (Beth et al., 1986; Anjaneylu et al., 1988, 1989). Most recently, a dihydrostilbene disulfonate derivative containing both a nitroxide and a reactive maleimide moiety has been developed, SL-H_2DADS-MAL (Wojcicki and Beth, 1993).

Important considerations related to the use of any probe molecule to investigate the global rotational diffusion of an integral membrane protein such as band 3 include the uniqueness of the label for band 3 in intact erythrocytes, the uniqueness of the reaction site of the label on band 3, the uniqueness of the orientation of the label with respect to the uniaxial rotational diffusion axis (assumed to be the membrane normal axis), and the amplitude of label motions caused by local or segmental motions of the protein or by local independent motions of the label itself. The available evidence demonstrates that SL-H_2DADS-MAL binds to, and reacts with, band 3 in intact erythrocytes with a very high specificity and that SL-H_2DADS-MAL and eosin-5-maleimide are mutually exclusive band-3-specific labels. Extensive studies carried out to date indicate that the spin-label moiety of SL-H_2DADS-MAL resides in a protected environment on band 3 and is inaccessible to both large hydrohilic and hydrophobic paramagnetic broadening agents (such as chromium oxalate, chromium maltolate, and $CuKTSM_2$ (2-keto-3-ethoxybutyraldehyde bis(N^4,N^4-dimethyl thiosemicarbazone) and to hydrophilic and hydrophobic chemical reducing agents (ascorbate and phenylhydrazine). The covalent reaction site of SL-H_2DADS-MAL has been localized to a 17-kDa integral membrane fragment of band 3 that is produced by chymotrypsin treatment of band 3 in intact cells, followed by mild trypsin treatment of ghost membranes. This is the same peptide that contains lysine-430, which has been shown to be the primary covalent reaction site of eosin-5-maleimide (Cobb and Beth, 1990). These findings strongly suggest a compact, highly protected, and geometrically unique labeling site. Preliminary reports of these results have appeared in abstract form (Wojcicki and Beth, 1993; Hustedt and Beth, 1994a,b; Scothorn et al., 1995); additional details of these and other results regarding the labeling of band 3 with SL-H_2DADS-MAL will be reported elsewhere (D. J. Scothorn, W. E. Wojcicki, E. J. Hustedt, A. H. Beth, and C. E. Cobb, manuscript in preparation).

Additional support for a unique labeling geometry has been obtained from the linear EPR spectra of [^{15}N,$^{2}H_{13}$]-SL-H_2DADS-MAL-labeled band 3 in intact erythrocytes that have been oriented by flow through a narrow-gap flat cell (Hustedt and Beth, 1994a,b). Analysis of these spectra, using two independent approaches, has provided a definition of the orientation of the nitroxide moiety with respect to the membrane normal axis in terms of a unique orientation. This result provides strong evidence against any large amplitude local motion of the nitroxide relative to band 3 or large amplitude segmental motion of the protein. Although it can be predicted that the global rotational motion of band 3 will be about the membrane normal axis, no such prediction can be made regarding any internal motions. It is more likely than not that any internal motion would be about an axis other than the membrane normal. Thus a local or segmental motion, if it were slow on the linear EPR time scale, would produce a distribution of nitroxide orientations relative to the membrane normal. More rapid nitroxide motions can also be ruled out given the narrow linewidths observed in the well resolved linear EPR spectrum of [^{15}N,$^{2}H_{13}$]-SL-H_2DADS-MAL-labeled band 3 in isotropically oriented intact erythrocytes (Hustedt and Beth, manuscript in preparation).

The results presented in Figs. 9 and 10 demonstrate that uniaxial rotational diffusion is a reasonable model to describe the rotational dynamics of band 3 in intact erythrocyte membranes at 37°C. Excellent fits to a uniaxial diffusion model were obtained from a simultaneous analysis of ST-EPR spectra obtained by using 100-, 50-, and 25-kHz Zeeman modulation frequencies. Good fits were also obtained, in Fig. 11, by using an isotropic rotational diffusion model. Clearly, isotropic rotational diffusion is not a plausible model for the global rotational dynamics of the transmembrane domain of band 3. However, X-band ST-EPR spectra for $\tau_{\|} \approx 10$ μs and $\theta \approx 30°$ are essentially indistinguishable from those obtained for an isotropic rotational diffusion model with $\tau_{iso} \approx 100$ μs (calculations not shown). It is important to emphasize that additional work remains to be done to determine the validity of the simple uniaxial rotation model to account for the rotational dynamics of band 3 in the erythrocyte membrane as observed by both ST-EPR and time-resolved anisotropy decay techniques.

One factor that determines the sensitivity of ST-EPR lineshapes to the rotational diffusion model is the orientation of the label with respect to the unique diffusion axis. As has been discussed by Beth and Robinson (1989), X-band ST-EPR spectra of a nitroxide undergoing uniaxial rotational diffusion will differ most dramatically from those for the isotropic rotational diffusion

model when $\theta \approx 0°$ or $\theta \approx 90°$. For intermediate labeling geometries where θ approaches the magic angle, X-band ST-EPR spectra for the uniaxial rotational diffusion model will be very similar to ST-EPR spectra for the isotropic rotational diffusion model for some effective isotropic rotational correlation time, $\tau_{iso} > \tau_{\|}$ (Beth and Robinson, 1989). The range of θ values over which it is difficult to distinguish at X-band between uniaxial and isotropic rotational diffusion models has not been systematically explored and will depend in part on the signal-to-noise ratio of the data being analyzed. It is likely that the use of higher microwave frequencies, such as Q-band, will help to discriminate between uniaxial rotational diffusion and other possible dynamic models. Studies of the rotational dynamics of [^{15}N,^{2}H$_{13}$]-SL-H$_2$DADS-MAL-labeled band 3 in erythrocyte membranes at Q-band (approximately 34 GHz) are now underway.

In previous time-resolved optical anisotropy studies of eosin-labeled band 3, the interpretation of various decay components in terms of distinct molecular species has remained ambiguous (Matayoshi and Jovin, 1991). It is clear that the fastest anisotropy decay components, in the range of 10 to 30 μs (Matayoshi and Jovin, 1991; McPherson et al., 1992), are within the range expected for a band 3 dimer. However it has not been possible from the optical anisotropy studies alone to determine whether these fast decays arise from a fraction of the total band 3. The results obtained in this work strongly suggest that all copies of band 3 exhibit a relatively large amplitude rotational mode that dominates the ST-EPR spectra and that is consistent with a band 3 dimer. It is important to consider the sensitivity of ST-EPR spectra to the rms amplitude of rotation. As noted above, the work of Howard et al. (1993) has shown that a rms amplitude of 10 to 90°, depending on correlation time, is sufficient to achieve the full saturation transfer effect. Thus, populations of band 3 that differ substantially in the extent to which their rotational motion is restricted cannot be ruled out. Given the known interactions between the cytoplasmic tail of band 3 and the membrane cytoskeleton, a population of band 3 whose rotational diffusion is restricted in amplitude is a reasonable expectation. Additional studies are underway to study the effect of various proteolytic cleavages and other experimental factors on the rotational dynamics of [^{15}N,^{2}H$_{13}$]-SL-H$_2$DADS-MAL-labeled band 3 as observed by ST-EPR. The initial studies presented here are intended to demonstrate that the [^{15}N,^{2}H$_{13}$]-SL-H$_2$DADS-MAL label and the computational algorithms outlined above make ST-EPR a valuable complementary spectroscopic technique for understanding of band 3 rotational dynamics and for clarifying the interpretion of time-resolved anisotropy decays of eosin-labeled band 3. Moreover, these same algorithms should be of general utility to investigators wishing to analyze ST-EPR data obtained from other integral membrane proteins.

APPENDIX

The following complete the definitions of all vectors and matrices of Eq. 14. One has

$$C_{0,1} = \begin{pmatrix} 0 & 0 & +\gamma_e h_m & 0 & 0 & 0 \\ -\gamma_e h_m & 0 & 0 & 0 & 0 & 0 \\ 0 & 0 & 0 & 0 & 0 & 0 \end{pmatrix} \qquad (31)$$

$$C_{1,0} = \begin{pmatrix} 0 & +\gamma_e h_m/2 & 0 \\ 0 & 0 & 0 \\ -\gamma_e h_m/2 & 0 & 0 \\ 0 & 0 & 0 \\ 0 & 0 & 0 \\ 0 & 0 & 0 \end{pmatrix}$$

and

$$C_{j,k} = \begin{pmatrix} 0 & 0 & +\gamma_e h_m/2 & 0 & 0 & 0 \\ 0 & 0 & 0 & +\gamma_e h_m/2 & 0 & 0 \\ -\gamma_e h_m/2 & 0 & 0 & 0 & 0 & 0 \\ 0 & -\gamma_e h_m/2 & 0 & 0 & 0 & 0 \\ 0 & 0 & 0 & 0 & 0 & 0 \\ 0 & 0 & 0 & 0 & 0 & 0 \end{pmatrix} \qquad (32)$$

for j,k both greater than zero. Also,

$$W_0^n = \begin{pmatrix} -R_{2e} & +\Delta^n & 0 \\ -\Delta^n & -R_{2e} & +\gamma_e h_1 \\ 0 & -\gamma_e h_1 & -R_{1e} \end{pmatrix} \qquad S_0^n = \begin{pmatrix} U_0^n \\ V_0^n \\ M_0^n \end{pmatrix} \qquad (33)$$

$$Q_0^n = \begin{pmatrix} 0 \\ 0 \\ (\omega_0 + \Delta^R)/T_{1e} \end{pmatrix}$$

and

$$W_k^n = \begin{pmatrix} -R_{2e} & -k\omega_m & +\Delta^n & 0 & 0 & 0 \\ +k\omega_m & -R_{2e} & 0 & +\Delta^n & 0 & 0 \\ -\Delta^n & 0 & -R_{2e} & -k\omega_m & +\gamma_e h_1 & 0 \\ 0 & -\Delta^n & +k\omega_m & -R_{2e} & 0 & +\gamma_e h_1 \\ 0 & 0 & -\gamma_e h_1 & 0 & -R_{1e} & -k\omega_m \\ 0 & 0 & 0 & -\gamma_e h_1 & +k\omega_m & -R_{1e} \end{pmatrix} \qquad (34)$$

$$S_k^n = \begin{pmatrix} U_k^n \\ U_k^n{}' \\ V_k^n \\ V_k^n{}' \\ M_k^n \\ M_k^n{}' \end{pmatrix} \qquad Q_k^n = \begin{pmatrix} 0 \\ 0 \\ 0 \\ 0 \\ (\gamma_e h_m)\delta_{1,k}/T_{1e} \\ 0 \end{pmatrix}$$

for k greater than zero. Finally, $R_{1e} = 1/T_{1e}$, $R_{2e} = 1/T_{2e}$, and Δ^n is given by Eq. 3 for a particular value of ϕ^n.

We are grateful to Dr. Bruce H. Robinson for many helpful discussions concerning the calculation of ST-EPR spectra and to Dr. Robinson and Scott M. Blackman for critically reviewing this manuscript before submission.

This work was supported by grants from the National Institutes of Health (HL 34737 and RR04075). E. J. H. has been supported by National Institutes of Health training grant T32 DK07186.

REFERENCES

Anjaneyulu, P. S. R., A. H. Beth, C. E. Cobb, S. F. Juliao, B. J. Sweetman, and J. V. Staros. 1989. Bis(sulfo-*N*-succinimidyl) doxyl-2-spiro-5′-azelate: synthesis, characterization, and reaction with the anion-exchange channel in intact human erythrocytes. *Biochemistry.* 28: 6583–6590.

Anjaneyulu, P. S. R., A. H. Beth, B. J. Sweetman, L. A. Faulkner, and J. V. Staros. 1988. Bis(sulfo-*N*-succinimidyl) [^{15}N,$^{2}H_{16}$]doxyl-2-spiro-5′-pimelate, a stable isotope-substituted, membrane impermeant bifunctional spin label for studies of the dynamics of membrane proteins: applications to the anion-exchange channel in intact human erythrocytes. *Biochemistry.* 27:6844–6851.

Balasubramanian, K., and L. R. Dalton. 1979. Computer simulation of EPR and ST-EPR spectra of nitroxide spin labels in the rigid-lattice limit. *J. Magn. Res.* 33:245–260.

Beechem, J. M., E. Gratton, M. Ameloot, J. R. Knutson, and L. Brand. 1991. The global analysis of fluorescence intensity and anisotropy decay data: second-generation theory and programs. *In* Topics in Fluorescence Spectroscopy, Vol. 2: Principles. J. R. Lakowicz, editor. Plenum Press, New York. 241–305.

Beth, A. H., K. Balasubramanian, B. H. Robinson, L. R. Dalton, S. D. Venkataramu, and J. H. Park. 1983. Sensitivity of V_2' saturation transfer electron paramagnetic resonance signals to anisotropic rotational diffusion with [^{15}N]nitroxide spin-labels, effects of noncoincident magnetic and diffusion tensor principal axes. *J. Phys. Chem.* 87: 359–367.

Beth, A. H., T. E. Conturo, S. D. Venkataramu, and J. V. Staros. 1986. Dynamics and interactions of the anion channel in intact human erythrocytes: an electron paramagnetic resonance spectroscopic study employing a new membrane-impermeant bifunctional spin-label. *Biochemistry.* 25:3824–3832.

Beth, A. H., and B. H. Robinson. 1989. Nitrogen-15 and deuterium substituted spin labels for studies of very slow rotational motion. *In* Biological Magnetic Resonance, Vol. 8: Spin Labeling Theory and Applications. L. J. Berliner and J. Reuben, editors. Plenum Press, New York. 179–249.

Cherry, R. J., A. Bürkli, M. Busslinger, G. Schneider, and G. R. Parish. 1976. Rotational diffusion of band 3 proteins in the human erythrocyte membrane. *Nature.* 263:389–393.

Cherry, R. J., and R. E. Godfrey. 1981. Anisotropic rotation of bacteriorhodopsin in lipid membranes. *Biophys. J.* 36:257–276.

Cobb, C. E., and A. H. Beth. 1990. Identification of the eosinyl-5-maleimide reaction site on the human erythrocyte anion-exchange protein: overlap with the reaction sites of other chemical probes. *Biochemistry.* 29:8283–8290.

Corbett, J. D., and D. E. Golan. 1993. Band 3 and glycophorin are progressively aggregated in density-fractionated sickle and normal red blood cells. *J. Clin. Invest.* 91:208–217.

Dalton, L. R. 1985. EPR and Advanced EPR Studies of Biological Systems. CRC Press, Boca Raton, FL. 314 pp.

Delmelle, M., K. W. Butler, and I. C. P. Smith. 1980. Saturation transfer electron spin resonance spectroscopy as a probe of anisotropic motion in model membrane systems. *Biochemistry.* 19:698–704.

Edmonds, A. R. 1957. Angular Momentum in Quantum Mechanics. Princeton University Press, Princeton, NJ. 146 pp.

Fajer, P., and D. Marsh. 1983. Sensitivity of saturation transfer ESR spectra to anisotropic rotation: application to membrane systems. *J. Magn. Res.* 51:446–459.

Freed, J. H. 1976. Theory of slow tumbling ESR spectra for nitroxides. *In* Spin Labeling Theory and Applications. L. J. Berliner, editor. Academic Press, New York. 53–132.

Gaffney, B. J. 1979. Spin label-thiourea adducts: a model for saturation transfer EPR studies of slow anisotropic rotation. *J. Phys. Chem.* 83: 3345–3349.

Ge, M., D. E. Budil, and J. H. Freed. 1994. ESR studies of spin-labeled membranes aligned by isopotential spin-dry ultracentrifugation: lipid-protein interactions. *Biophys. J.* 67:2326–2344.

Hemminga, M. A., and P. A. de Jager. 1989. Saturation transfer spectroscopy of spin labels: techniques and interpretation of spectra. *In* Biological Magnetic Resonance, Vol. 8: Spin Labeling Theory and Applications. L. J. Berliner and J. Reuben, editors. Plenum Press, New York. 179–249.

Howard, E. C., K. M. Lindahl, C. F. Polnaszek, and D. D. Thomas. 1993. Simulation of saturation transfer electron paramagnetic resonance spectra for rotational motion with restricted angular amplitude. *Biophys. J.* 64:581–593.

Hustedt, E. J., and A. H. Beth. 1994a. The determination of the orientation of a nitroxide spin-label relative to band 3 protein of the human red blood cell. *Biophys. J.* 66:A41.

Hustedt, E. J., and A. H. Beth. 1994b. The rotational diffusion of band 3 in intact red blood cell membranes as measured by saturation transfer EPR spectroscopy. *Biophys. J.* 66:A42.

Hustedt, E. J., C. E. Cobb, A. H. Beth, and J. M. Beechem. 1993. Measurement of rotational dynamics by the simultaneous nonlinear analysis of optical and EPR data. *Biophys. J.* 64:614–621.

Hustedt, E. J., J. J. Kirchner, A. Spaltenstein, P. B. Hopkins, and B. H. Robinson. 1995. Monitoring DNA dynamics using spin-labels with different independent mobilities. *Biochemistry.* 34:4369–4375.

Hyde, J. S., and L. R. Dalton. 1972. Very slow tumbling spin labels: adiabatic rapid passage. *Chem. Phys. Lett.* 16:568–572.

Hyde, J. S., and L. R. Dalton. 1979. Saturation transfer spectroscopy. *In* Spin Labeling II: Theory and Applications. L. J. Berliner, editor. Academic Press, New York. 1–70.

Isaacson, E., and H. B. Keller. 1966. Analysis of Numerical Methods. John Wiley & Sons, New York. 541 pp.

Jähnig, F. 1986. The shape of a membrane protein derived from rotational diffusion. *Eur. Biophys. J.* 14:63–64.

Matayoshi, E. D., and T. M. Jovin. 1991. Rotational diffusion of band 3 in erythrocyte membranes. I. comparison of ghosts and intact cells. *Biochemistry.* 30:3527–3538.

McCalley, R. C., E. J. Shimshick, and H. M. McConnell. 1972. The effect of slow rotational motion on paramagnetic resonance spectra. *Chem. Phys. Lett.* 13:115–119.

McCaughan, L., and S. Krimm. 1980. X-ray and neutron scattering density profiles of the intact human red blood cell membrane. *Science.* 207: 1481–1483.

McPherson, R. A., W. H. Sawyer, and L. Tilley. 1992. Rotational diffusion of the erythrocyte integral membrane protein band 3: effect of hemichrome binding. *Biochemistry.* 31:512–518.

McPherson, R. A., W. H. Sawyer, and L. Tilley. 1993. Band 3 mobility in camelid elliptocytes: implications for erythrocyte shape. *Biochemistry.* 32:6696–6702.

Nigg, E., and R. J. Cherry. 1979. Dimeric association of band 3 in the erythrocyte membrane demonstrated by protein diffusion measurements. *Nature.* 277:493–494.

Robinson, B. H. 1983. Effect of overmodulation on saturation transfer EPR signals. *J. Chem. Phys.* 78:2268–2273.

Robinson, B. H., and L. R. Dalton. 1980. Anisotropic rotational diffusion studied by passage saturation transfer electron paramagnetic resonance. *J. Chem. Phys.* 72:1312–1324.

Saffman, P. G., and M. Delbrück. 1975. Brownian motion in biological membranes. *Proc. Natl. Acad. Sci. USA.* 72:3111–3113.

Schneider, D. J., and J. H. Freed. 1989. Calculating slow motional magnetic resonance spectra: a user's guide. *In* Biological Magnetic Resonance, Vol. 8: Spin Labeling Theory and Applications. L. J. Berliner and J. Reuben, editors. Plenum Press, New York. 1–76.

Scothorn, D. J., E. J. Hustedt, C. E. Cobb, and A. H. Beth. 1995. Local environment of two structurally distinct spin-labeled affinity probes of human erythrocyte band 3. *Biophys. J.* 68:A305.

Squier, T. C., and D. D. Thomas. 1986. Methodology for increased precision in saturation transfer electron paramagnetic resonance studies of rotational dynamics. *Biophys. J.* 49:921–935.

Thomas, D. D. 1985. Saturation transfer EPR studies of microsecond rotational motions in biological membranes. *In* The Enzymes of Biological Membranes, Vol. 2, 2nd ed. A. N. Martonosi, editor. Plenum Press, New York. 287–312.

Thomas, D. D. 1986. Rotational diffusion of membrane proteins. *In* Techniques for the Analysis of Membrane Proteins. C. I. Ragan and R. J. Cherry, editors. Chapman and Hall, London. 377–431.

Thomas, D. D., L. R. Dalton, and J. S. Hyde. 1976. Rotational diffusion studied by passage saturation transfer electron paramagnetic resonance. *J. Chem. Phys.* 65:3006–3024.

Thomas, D. D., and H. M. McConnell. 1974. Calculation of paramagnetic resonance spectra sensitive to very slow rotational motion. *Chem. Phys. Lett.* 25:470–475.

Tsuji, A., K. Kawasaki, S.-I. Ohnishi, H. Merkle, and A. Kusumi. 1988. Regulation of band 3 mobilities in erythrocyte ghost membranes by protein association and cytoskeletal meshwork. *Biochemistry.* 27: 7447–7452.

van der Meer, B. W. 1993. Fluidity, dynamics and order. *In* Biomembranes, Physical Aspects. M. Shinitzky, editor. VCH Inc., New York. 97–158.

Wang, D. N., W. Kühlbrandt, V. E. Sarabia, and R. A. F. Reithmeier. 1993. Two-dimensional structure of the membrane domain of human band 3, the anion transport protein of the erythrocyte membrane. *EMBO J.* 12:2233–2239.

Wang, D. N., V. E. Sarabia, R. A. F. Reithmeier, and W. Kühlbrandt. 1994. Three-dimensional map of the dimeric membrane domain of the human erythrocyte anion exchanger, band 3. *EMBO J.* 14:3230–3235.

Wojcicki, W. E., and A. H. Beth. 1993. Spin-labeled H_2-DADS-maleimide, a new probe for the study of erythrocyte membrane protein dynamics using EPR spectroscopy. *Biophys. J.* 64:A308.